The Extinction Spectra of Silver Nanoparticle Arrays: Influence of Array Structure on Plasmon Resonance Wavelength and Width†

LinLin Zhao, K. Lance Kelly, and George C. Schatz*

Department of Chemistry, Northwestern University, Evanston, Illinois 60208-3113

Received: January 29, 2003; In Final Form: March 18, 2003

We use high-quality electrodynamics methods to study the extinction spectra of one-dimensional linear chains and two-dimensional planar arrays of spherical silver nanoparticles, placing emphasis on the variation of the plasmon resonance wavelength and width with array structure (spacing, symmetry), particle size, and polarization direction. Two levels of theory have been considered, coupled dipoles with fully retarded interactions and T-matrix theory that includes a converged multipole expansion on each particle. We find that the most important array effects for particles having a radius of 30 nm or smaller are captured by the couple dipole approach. Our calculations demonstrate several surprising effects that run counter to conventional wisdom in which the particle interactions are assumed to be governed by electrostatic dipolar interactions. In particular, we find that for planar arrays of particles with polarization parallel to the plane the plasmon resonance blue shifts as array spacing D decreases for D larger than about 75 nm and then it red shifts for smaller spacings. In addition, we find that the plasmon narrows for $D > 180$ nm but broadens for smaller spacings. The results can be rationalized using a simple analytical model, which demonstrates that the plasmon wavelength shift is determined by the real part of the retarded dipole sum while the width is determined by the imaginary part of this sum. The optimal blue shifts and narrowing are found when the particle spacing is slightly smaller than the plasmon wavelength, while red shifts and broadening can be found for spacings much smaller than the plasmon wavelength at which electrostatic interactions are dominant. We also find that the array spectrum does not change significantly with array symmetry (square or hexagonal) or irradiated spot size (i.e., constant array size or constant particle number).

I. Introduction

Well-defined nanoparticle arrays and aggregates provide opportunities for observing interesting, new, and potentially useful collective optical phenomena. Recently, new classes of chemical, biological, and optical sensors have been produced using silver or gold nanoparticles, in which aggregation-induced electromagnetic interactions between the particles results in a color change that signals detection.[1] The plasmon resonance optical properties of nanometer colloidal-gold nanoparticles have also been used in bioconjugates, biochips, and biosensors.[1,2] Plasmon coupling along a chain of particles has been proposed for energy transport in subwavelength structures, and as a result, light signal routers, "nanoantennas",[3,4] have been constructed that can be selectively driven into a dipolar or quadrupolar oscillation pattern. High-resolution scanning surface plasmon microscopies[5,6] and polarizing optical filters[7,8] have also been designed.

These new experimental studies provide important challenges to classical electrodynamics theory. In the past few years, researchers have developed several numerical methods for describing nanoparticle arrays and aggregates that have complex structures, including the discrete dipole approximation (DDA),[9,10] the multiple multipole method (MMP),[11] the finite difference time domain method (FDTD),[12] and the T-matrix method.[13] The DDA method (also called the volume discretization method) divides the object into a large number of polarizable cubes. The induced dipole polarizations in these cubes are determined self-consistently, and then optical properties are determined using the induced polarizations. The MMP method separates the field domain into a number of subdomains and then solves the differential equations in each subdomain analytically and matches boundary conditions between different domains numerically, that is, via least-squares fitting. FDTD methods discretize the entire volume of the scatterer to numerous Yee cells and then solve Maxwell's equations as a function of time numerically. The T-matrix method expresses the fields inside and outside the object as expansions in vector spherical harmonics and then does exact matching within the subspace of the spherical harmonic basis by projecting the matching equations onto the basis. An overview of these and other methods can be found elsewhere.[14,15] These numerical methods have enabled the computations of surface plasmon resonances for complex geometrical configurations and the inclusion of particle interactions at a high level.[16,17]

In this paper, we are interested in light scattering from one-dimensional linear chains and two-dimensional arrays with the goal of determining the influence of electromagnetic coupling between particles over a wide range of particle spacings and for a broad range of array structures. Numerous experiments show that the optical spectra of arrays and aggregates are influenced by particle shape and size,[18−20] interactions between neighboring particles,[21−23] and polarization of the incident light,[24,25] but a general understanding of how these factors influence extinction spectra has not been developed. When the interparticle distance is comparable to or less than the particle size, the interactions between particles play a significant role in the optical response.[26,27] Often these interactions are interpreted using electrostatic concepts, wherein the interaction of

† Part of the special issue "Arnim Henglein Festschrift".

10.1021/jp034235j CCC: $25.00
Published on Web 05/01/2003

parallel collinear dipoles typically leads to red-shifting of the plasmon wavelengths, while parallel but noncollinear dipoles produce blue-shifted plasmon wavelengths.

Also, for planar arrays of dipoles, it is well-known that electrostatic dipolar interactions lead to red-shifted resonance response.[28] However for particle spacings of $\lambda/(2\pi)$ or more (i.e., >70 nm), long-range electrodynamic interactions are important, and these, as we will show, change the effect of particle interaction in dramatic ways compared to electrostatic theory. Our goal, then, is to determine what these effects are and how they vary with array structure so that we ultimately might design arrays for sensor applications in which the influence of array structure on array spectra is used for detection.

A convenient way to study electromagnetic interactions in arrays of spherical particles is to use the T-matrix method (or coupled multipole method). It is restricted to clusters with nonoverlapping spheres or spheroidal particles, and the extinction cross section of the clusters is calculated from a solution to Maxwell's equations that is exact except for the use of a truncated multipolar expansion around each particle. The computational effort associated with this approach depends on the number of particles, the interparticle distances, and the maximum order multipole included in the calculation, and it can be quite substantial when many closely spaced particles are present.[29] Despite this significant expense, T-matrix theory produces essentially exact results that are useful for benchmarking simpler methods, such as the coupled dipole approximation (CD).[30]

The latter approach (CD) is just the T-matrix method in which only dipole fields are used to describe each particle in the array. The underlying CD theory is formally similar to DDA; however, in CD, one represents each particle by a single dipole of which the polarizability is simply that of the particle, while in DDA, one represents each particle by a grid of polarizable dipoles of which the polarizability is determined by a lattice dispersion formula that is designed to make the response of the dipole array be identical to that of bulk continuum. Previous work[31] has shown that, if the particles in the CD calculation are assumed to be located on a cubic lattice (not all lattice sites need to be occupied), then we can efficiently evaluate the dipole sums using Fourier methods and thereby calculate the optical properties of arrays with a much larger number of particles (up to 10^5), which can be done with real-space solutions and with much less computational effort relative to that associated with the T-matrix method. This lattice-based approach makes the CD and DDA calculations functionally the same except for the difference in polarizabilities of the lattice points.

We consider both the T-matrix and CD approaches in the present application, and we further examine simple semianalytical approaches, which make it possible to interpret the results using simple concepts. In a companion paper,[32] the results of measurements are presented which test many of the qualitative and semiquantitative concepts developed here.

The paper is organized as follows. In section II, we describe the methods for the numerical calculation of the extinction spectra. Section III describes the geometry of the clusters used and the corresponding results of numerical simulations and provides a semianalytical approach for infinite two-dimensional arrays. Section IV summarizes our results.

II. Electrodynamics Methods

A. Coupled Dipole Approximation (CD). The behavior of light incident on a macroscopic target is governed by Maxwell's equations for the electric and magnetic vector fields. The general framework for modeling the optical response of a collection of spheres involves self-consistent solution of the response of each particle to the incident field and the scattered fields of the other particles. Here, we assume that all of the particles are coherently excited. Spherical particles of nonmagnetic materials with sizes much smaller than the wavelength of light respond primarily to the electric dipole component of the local field. Therefore, as long as the component nanospheres are not spaced too closely, the response of an aggregate to electromagnetic radiation can be determined by self-consistent solution of the electric dipole polarizations, $\mathbf{P}_i$, of each sphere in the field of the incident light and the sum of the dipole fields of the other particles. Thus if we assume that we have N polarizable particles and that the ith particle has a polarizability α_i (and no higher multipole polarizabilities) and has its center at a position denoted $\mathbf{r}_i$, then for a given dipole at position $\mathbf{r}_i$,

$$\mathbf{P}_i = \alpha \cdot \mathbf{E}_{\mathrm{loc}}(\mathbf{r}_i) \tag{1}$$

where $\mathbf{E}_{\mathrm{loc}}(\mathbf{r}_i)$ is the sum of an incident field, $\mathbf{E}_{\mathrm{inc},i} = \mathbf{E}_0\, e^{ik\mathbf{r}_i}$, and the retarded fields of the other $N-1$ dipoles. These fields are given by (for $k = 2\pi/\lambda$)

$$\mathbf{E}_{\mathrm{loc}}(\mathbf{r}_i) = \mathbf{E}_0\, e^{ik\mathbf{r}_i} + \sum_{j=1} \frac{e^{ik\mathbf{r}_{ij}}}{\mathbf{r}_{ij}^{\,3}} \left\{ k^2 \mathbf{r}_{ij} \times (\mathbf{r}_{ij} \times \mathbf{P}_j) + \frac{1 - ik\mathbf{r}_{ij}}{\mathbf{r}_{ij}^{\,2}} \times [\mathbf{r}_{ij}^{\,2}\mathbf{P}_j - 3\mathbf{r}_{ij}(\mathbf{r}_{ij}\cdot\mathbf{P}_j)] \right\} \tag{2}$$

where $\mathbf{r}_{ij}$ is the vector between the ith and jth particles (with $r_{ij} = |\mathbf{r}_{ij}|$). Substituting eq 2 into eq 1 and rearranging terms, we generate an equation of the form

$$(\alpha^{-1})\mathbf{P}_i + \sum_{j \neq i} \mathbf{A}_{ij} \cdot \mathbf{P}_j = \mathbf{E}_{\mathrm{inc},i} \quad \text{or} \quad \mathbf{A}'\mathbf{P} = \mathbf{E}_{\mathrm{inc}} \tag{3}$$

where $\mathbf{A}_{ij}$ is the matrix of coefficients in eq 2. In the second form of eq 3, $\mathbf{P}$ and $\mathbf{E}_{\mathrm{inc}}$ are $3N$ vectors and $\mathbf{A}$ is a $3N \times 3N$ symmetric matrix constructed from the 3×3 interparticle interaction matrices $\mathbf{A}_{ij}$ with additional terms α^{-1} along the diagonal. Solving this set of $3N$ complex linear equations allows the polarization vector $\mathbf{P}$ to be obtained and, consequently, the optical properties to be calculated. For the extinction cross section that we are interested in, it is calculated using

$$C_{\mathrm{ext}} = \frac{4\pi k}{|\mathbf{E}_{\mathrm{inc}}|^2} \sum_{j=1}^{N} \mathrm{Im}\{\mathbf{E}_{\mathrm{inc},j}^{*} \cdot \mathbf{P}_j\} \tag{4}$$

Note that the dipole field in eq 2 consists of two parts, the second of which varies as $1/r^3$ for small r and the first of which varies as $1/r$. The second part includes the familiar $(3\cos^2\theta - 1)/r^3$ that we would expect from electrostatics, while the first term is the radiative dipole field that varies as $\sin^2\theta/r$. Both terms are modulated by the factor $e^{ik\mathbf{r}}$, such that when $\mathbf{r}$ is comparable to or larger than $\lambda/(2\pi)$, that is, >60−120 nm for plasmon resonances in the visible, the field is strongly modulated from its electrostatic values and can even change sign. Later we will see that these two factors, that is, the radiative dipole term and the $e^{ik\mathbf{r}}$ factor, can in some cases lead to major changes in the electrodynamic response of an array relative to what would be expected on the basis of electrostatics.

B. T-Matrix Method. The T-matrix method is an exact technique for simulating light scattering by particle arrays based on Mie theory for each particle and the translation addition

theorem for vector spherical harmonics.[23,33−37] It was initially developed by Waterman[38] and has been significantly improved by Mishchenko and co-workers.[39−43] The procedure of analytically calculating the T-matrix for a cluster of spheres has been described in detail in ref 37, and a general review of this approach can be found in ref 43.

In the following, we give the basic idea of this approach. Consider a cluster of N arbitrarily shaped scattering particles illuminated by a plane incident electromagnetic wave. The scattered field from the cluster as a whole can be given as a superposition of partial fields scattered from each of the N_s spheres in the cluster, that is,

$$\mathbf{E}_s = \sum_{i=1}^{N_s} \mathbf{E}_{s,i} \tag{5}$$

where each partial field $\mathbf{E}_{s,i}$, in turn, is represented by an expansion of vector spherical harmonics centered about the origin of the ith sphere,

$$\mathbf{E}_{s,i} = \sum_{n=1}^{\infty} \sum_{m=-np=1}^{n} \sum^{2} a^i_{mnp} \mathbf{h}_{mnp}(\mathbf{r}_i) \tag{6}$$

Here, $\mathbf{h}$ denotes the outgoing wave vector spherical harmonics of order n and degree m; a^i are the corresponding scattered-field expansion coefficients for sphere i, and p denotes the modes of the scattered field, $p = 1$ and 2 referring to the TM and TE modes, respectively.

Because of the electromagnetic interactions between spheres in the cluster, the scattered field of the ith sphere consists of the incident field plus scattered fields originated from all other spheres. Invoking the addition theorem for vector harmonics, these interacting fields can be transformed into expansions about the origin of sphere i. Truncating the expansions (eq 6) to $n = N_{O,i}$ orders, one can obtain a system of equations for the scattering coefficients written as

$$a^i_{mnp} + \bar{a}^i_{np} \sum_{j=1,j\neq i}^{N_s} \sum_{l=1}^{N_{O,i}} \sum_{k=-1}^{l} \sum_{q=1}^{2} H^{ij}_{mnpklq} a^j_{klq} = \bar{a}^i_{np} p^i_{mnp} \tag{7}$$

in which the matrix H^{ij} is formed from the vector harmonic addition coefficients (based on the spherical Hankel functions) and only depends on the distance and the direction of translation from origins j to i, $\bar{a}^i$ are the Lorenz/Mie multipole scattering coefficients for sphere i, and p^i are the expansion coefficients for the plane, linearly polarized incident wave at the origin of i. Formal inversion of this system of equations gives the sphere-centered T-matrix of the cluster,

$$a^i_{mnp} = \sum_{j=1}^{N_s} \sum_{l=1}^{N_{O,i}} \sum_{k=-1}^{l} \sum_{q=1}^{2} T^{ij}_{mnpklq} p^j_{klq} \tag{8}$$

This sphere-centered T^{ij} can be transformed into an equivalent cluster-centered T-matrix that is based upon a single origin of the cluster.

$$T_{nl} = \sum_{i=1}^{N_s} \sum_{j=1}^{N_s} \sum_{n'=1}^{N_{O,i}} \sum_{l'=1}^{N_{O,i}} J^{0i}_{nn'} T^{ij}_{n'l'} J^{j0}_{l'l} \tag{9}$$

where J^{0i} and J^{j0} are matrices formed from the addition coefficients based on the spherical Bessel function and the subscripts n and l (and their primes) are shorthand for order, degree, and mode. Different kinds of cross sections in both fixed and random orientation can then be obtained from relatively simple operations directly on this T-matrix. For the extinction efficiency, its expression is

$$C_{ext} = \frac{2\pi}{k^2} \mathrm{Re}\left(\sum_{n,m,p} T_{mnpmnp}\right) \tag{10}$$

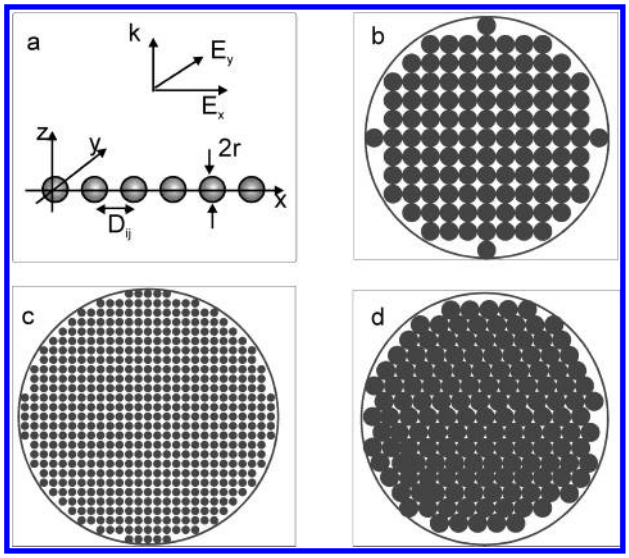

Figure 1. Structures of one-dimensional chain and two-dimensional array used in this work: (a) linear-chain structure and definition of the coordinate system; (b) square structure arranged in a circular shape, $N = 113$; (c) square structure arranged in circular shape, $R_{agg} = 1$ μm; (d) hexagonal structure arranged in circular shape, $R_{agg} = 1$ μm.

III. Results and Discussion

In the following sections, we present the results of our electrodynamics calculations, first for one-dimensional linear chains and then for the two-dimensional arrays. All particle clusters considered here are in a vacuum, and they are made of equal-sized and equally spaced spherical silver particles using dielectric constants from Palik.[44] The radii r of the component particles have been chosen to be 30 nm because particles of this size are commonly encountered in nanoparticle experiments and they are small enough that their surface plasmons are still of dipolar character but, at the same time, they are large enough that the above-mentioned electrodynamic corrections are important. Figure 1 shows the structures of the clusters and the definition of the coordinate system used in the calculations. The normal to the interparticle axis (the x axis for the one-dimensional linear chain) or the cluster surface (the $x-y$ plane for two-dimensional array) is set to be the z axis, and the plane of incidence is set to be the $x-z$ plane. Two kinds of polarization exist for the incident electric field: p-polarization for incident light polarized parallel to the plane of incidence and s-polarization for incident light polarized perpendicular to the plane of incidence. The array spacing D is the distance between the centers of the first nearest-neighbor particles. Often we will specify D in terms of its ratio to the sphere diameter, that is, $D/(2r)$. For each structure, we've studied the dependence of extinction spectra on interparticle distance and polarization directions. To show the importance of the particle size on the extinction spectra, we also consider clusters consisting of $r = 5$ nm spheres.

In the Introduction, we mentioned that one can perform CD calculations with the particles located on a lattice. We did not use this approach here because the number of particles that we studied (up to 1000) was such that the additional efficiencies

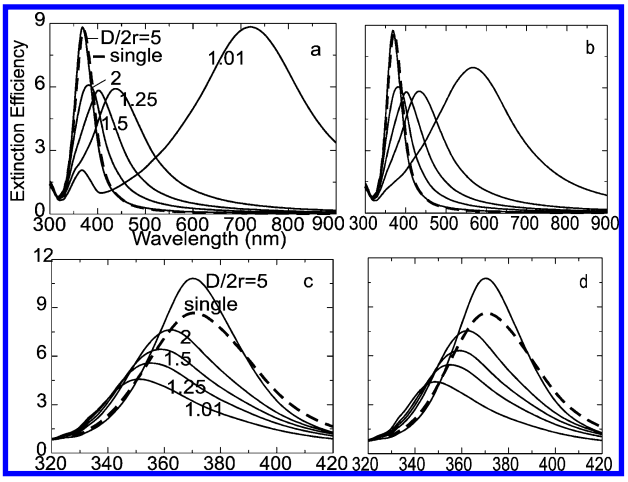

Figure 2. Variation of extinction spectrum for linear chain of 30-nm spheres with $D/(2r)$ chosen to be 5, 2, 1.5, 1.25, and 1.01: (a) T-matrix results for parallel polarization; (b) CD results for parallel polarization; (c) T-matrix results for perpendicular polarization; (d) CD results for perpendicular polarization. Also included in each plot is the result for a single sphere.

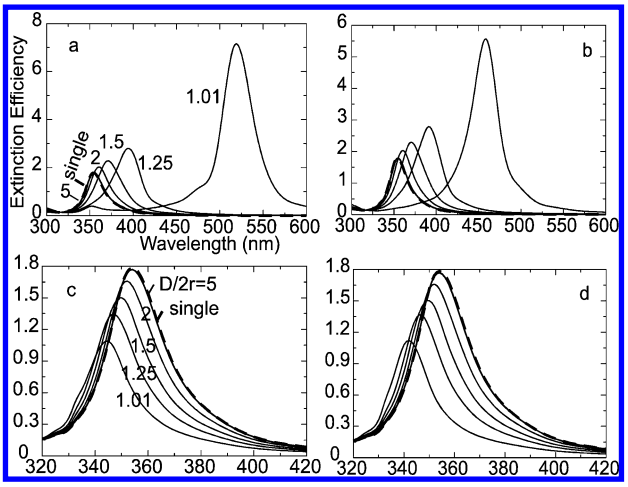

Figure 3. Variation of extinction spectrum for linear chain of 5-nm spheres with $D/(2r)$ set to be 5, 2, 1.5, 1.25, and 1.01: (a) T-matrix results for parallel polarization; (b) CD results for parallel polarization; (c) T-matrix results for perpendicular polarization; (d) CD results for perpendicular polarization. Also included in each plot is the result for a single sphere.

of the grid approach were not needed. In addition, we wanted to be able to place the particles at precisely the same coordinates as those used in the T-matrix calculations (which is not a grid-based approach). For arrays of 100 30-nm spherical nanoparticles that are separated by several diameters, the CPU time per wavelength is around 5 min (on a Sun workstation) for the T-matrix calculations, while for arrays of 1000 almost touching 30-nm spherical nanoparticles, the time per wavelength is at least 10 h. This is to be contrasted with times of 30 s and 3 h for the corresponding CD calculations.

A. One-Dimensional Linear Chains. We first consider the extinction spectra of one-dimensional linear chains, N, the number of the particles in the chain, being 100. Figures 2 and 3 present variations of extinction with separation ratio $D/(2r)$ for 30 and 5 nm spheres, respectively, for parallel and perpendicular polarizations. Also plotted is the extinction for a single sphere, which is the same as that having $D/(2r) = \infty$. In both figures, panels a and c present T-matrix multipole results and panels b and d presents the results of CD calculations. All results are presented as extinction efficiencies, which are the ratio of the calculated extinction cross section to the total cross-sectional area ($N\pi r^2$) of the particles in the chain.

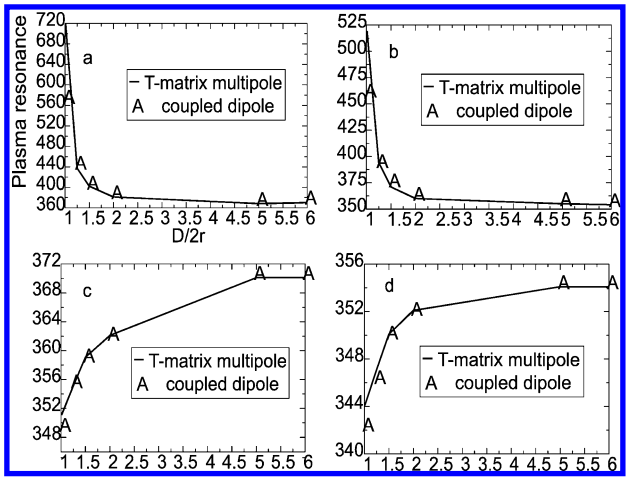

Figure 4. Plots of plasmon resonance wavelength versus $D/(2r)$: (a) parallel polarization, $r = 30$ nm; (b) parallel polarization, $r = 5$ nm; (c) perpendicular polarization, $r = 30$ nm; (d) perpendicular polarization, $r = 5$ nm.

Figure 4 presents the *dipole plasmon*[45] wavelength λ_{max} as a function of $D/(2r)$, panels a and b showing 30- and 5-nm sphere results for parallel polarization and panels c and d the 30- and 5-nm results for perpendicular polarization. The figure shows that particle size does not have much influence on the variation of λ_{max} as long as the response of the spheres is predominantly dipolar in character. Second and most important, the CD approach gives the same patten for the plasmon resonance shifts as the T-matrix method; that is, under parallel polarization, λ_{max} slightly blue shifts at first and then strongly red shifts as $D/(2r)$ decreases, while for perpendicular polarization, λ_{max} only blue shifts. This optical behavior can be understood in terms of the collective response of the coupled particles: under parallel polarization, the longitudinal[46] surface plasmon mode (associated with the interparticle axis) is excited and the dipole fields are all in phase leading to red shifts, whereas under perpendicular polarization, the transverse mode (associated with the short axis of the particle) is excited and the induced dipole fields are all out of phase, leading to blue shifts. The only exception to this arises in the slight blue shift seen in Figure 4a for parallel polarization at relatively large spacings ($D/(2r) = 5$). This spacing is sufficiently large (300 nm) that the $e^{ik\mathbf{r}}$ factor in eq 2 is close to -1, which means that the dipole fields now interact destructively rather than constructively and what would have been red shifts turns into blue shifts. Because this is a very minor point, we will not elaborate further, but later when we consider planar arrays, a related but more important issue will be considered.

Note that in Figure 2a, there is a second peak (at about 365 nm, likely corresponding to quadrupole excitation) in the extinction spectra for a separation ratio $D/(2r) = 1.25$ or 1.01, but in Figure 2b, this peak is smaller or even disappears completely. Moreover, Figure 4 shows that for these two ratios, λ_{max}'s obtained from the T-matrix method are more to the red than those from the CD approach. This means that when the spacing is comparable to or less than the component particle size, the dipole approximation is not adequate and high-order multipole moments, coupled both to each other and to the incident field, must be taken into account.

It has been suggested that to account for multipolar effects in the CD approach, one can replace the touching spheres by overlapping spheres, that is, set the ratio $D/(2r)$ less than 1. In

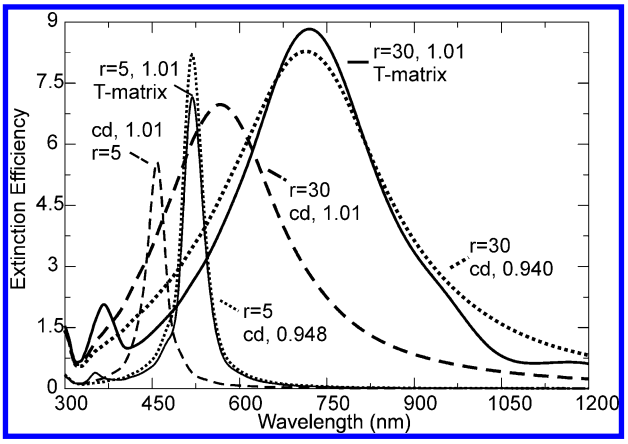

Figure 5. Extinction of one-dimensional chain using CD approach to simulate T-matrix multipole results for $D/(2r) = 1.01$ with $r = 30$ and 5 nm.

addition, it was shown[30,47,48] that for a linear chain of spheres, within the dipole approximation, the corrected ratio can be obtained by assuming equality of the total volume of the spheres and the chain as a whole, that is, $D/(2r) = ((4\pi/3)^{1/3})/2 = 0.806$. To test this hypothesis, in Figure 5, we present plots of extinction spectra for chains of 30- and 5-nm spheres with the original $D/(2r) = 1.01$. This figure shows that one can indeed simulate the T-matrix multipole results using the CD approach and a modified value of $D/(2r)$. However, the ratio should be chosen differently than has been used previously, that is, instead of $D/(2r) = 0.806$, one should choose $D/(2r) = 0.940$ or 0.948 for chains of 30- or 5-nm spheres for the most realistic behavior.

B.Two-Dimensional Arrays. In this section, we present results for two-dimensional square and hexagonal structures arranged in a circular pattern with a fixed particle number $N = 113$ (Figure 1b) or with a fixed array size $R_{agg} = 1\ \mu$m (Figure 1c,d). For each structure, the particle size has been chosen to be 30 nm. It has been pointed out that for clusters with a geometrical symmetry corresponding to that of the infinite array, the optical response is invariant with respect to any rotation about the z axis, while for finite clusters, optical anisotropy in the $x-y$ plane is expected.[49] For the square and hexagonal structures considered here, all of the calculations refer to normal incidence for which p- and s-polarization are identical for infinite arrays. For finite arrays, we choose the polarization to be along an axis that corresponds to the smallest interparticle spacing. Because all of the arrays considered have a large number of particles, the results of averaging over in-plane polarization directions are nearly identical.

Figure 6 presents T-matrix multipole results for (a) a square lattice structure with a fixed particle number, (b) a square structure with a fixed array size, and (c) a hexagonal structure with a fixed array size. Figure 6d shows λ_{max} versus $D/(2r)$ for these three systems. Figure 7 presents the same series of results as obtained from CD calculations. Comparing these two figures, we find that for two-dimensional arrays the most important array effects are captured by the CD approach. Both methods show that for a given array structure the extinction spectrum does not change with the measurement conditions (i.e., fixed *particle number* or fixed *array size*) and for a given measurement condition it does not change with array symmetry (i.e., *square* or *hexagonal*). More important, both calculations show that (a) the plasmon wavelength *blue shifts* as array spacing decreases for D larger than 75 nm and then *red shifts* for smaller distances and (b) the plasmon width narrows for $D > 180$ nm but broadens for smaller distances. Some aspects of this unusual optical

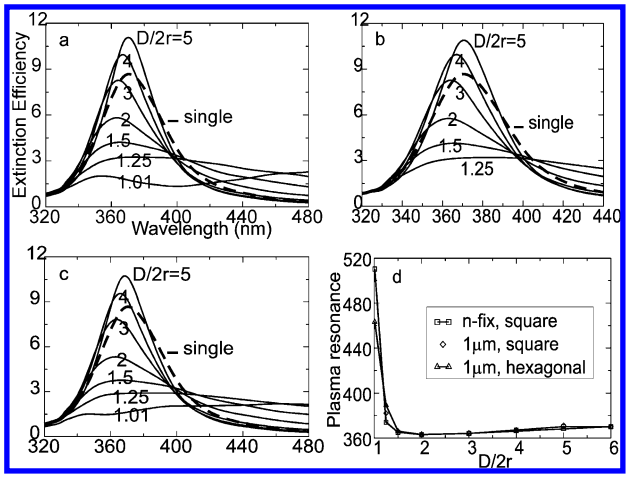

Figure 6. Variation of extinction for two-dimensional array of 30-nm spheres with different $D/(2r)$ obtained from T-matrix multipole calculation: (a) results for square structure, N fixed; (b) results for square structure, fixed array size; (c) results for hexagonal structure, fixed array size; (d) comparison of λ_{max} obtained for these three structures. Also included in each plot is the result for a single sphere. Note that a different wavelength scale is used in panels a−c.

behavior (the blue shifting and narrowing) have been found in related experimental work[50] for the 100 nm diameter particles that have separations comparable to what we are considering. In addition, in the companion to this paper,[32] blue shifting but not narrowing is found for disk-shaped particles.

C. A Simple Semianalytical Model. To qualitatively understand this behavior, here we examine a simple semianalytical model based on the coupled dipole treatment and an infinite array of particles.[9] Figure 8 presents the two-dimensional infinite array structure and the coordinate systems used in this model. (The model also applies to one-dimensional chains, and we will consider this case later on.) As with the CD approach, the polarization induced in the ith sphere is defined as $\mathbf{P}_i = \alpha_{cluster} \cdot \mathbf{E}_{loc,i}$, and $\mathbf{E}_{loc,i}$ is

$$\mathbf{E}_{loc,i} = \mathbf{E}_{app} + \sum_{j \neq i} \left[\frac{(1 - ik\mathbf{r}_{ij})(3\cos^2\theta_{ij} - 1)\, e^{ik\mathbf{r}_{ij}}}{\mathbf{r}_{ij}^{\,3}} + \frac{k^2 \sin^2\theta_{ij}\, e^{ik\mathbf{r}_{ij}}}{\mathbf{r}_{ij}} \right] (\alpha_s \cdot \mathbf{E}_{loc,j}) \quad (11)$$

where $\mathbf{r}_{ij}$ is the vector between the ith and jth spheres (with $r_{ij} = |\mathbf{r}_{ij}|$), θ_{ij} is the angle between $\mathbf{r}_{ij}$ and the polarization direction, and α_s is the single-sphere polarizability. For an infinite array being irradiated normal to the plane, one can assume that the local e-fields of all spheres are the same (i.e., $\mathbf{E}_{loc,i} = \mathbf{E}_{loc,j} = \mathbf{E}_{loc}$) and rearrange the above equation to $\mathbf{E}_{loc} = \mathbf{E}_{app}/(1 - \alpha_s S)$. Thus the effective polarizability of the whole array and the extinction cross section are given by

$$\alpha_{cluster} = \frac{\alpha_s}{1 - \alpha_s S} \quad \text{and} \quad C_{ext} = 4\pi k\, \mathrm{Im}(\alpha_{cluster}) \quad (12)$$

S being the retarded dipole sum

$$S = \sum_{j \neq i} \left[\frac{(1 - ik\mathbf{r}_{ij})(3\cos^2\theta_{ij} - 1)\, e^{ik\mathbf{r}_{ij}}}{\mathbf{r}_{ij}^{\,3}} + \frac{k^2 \sin^2\theta_{ij}\, e^{ik\mathbf{r}_{ij}}}{\mathbf{r}_{ij}} \right] \quad (13)$$

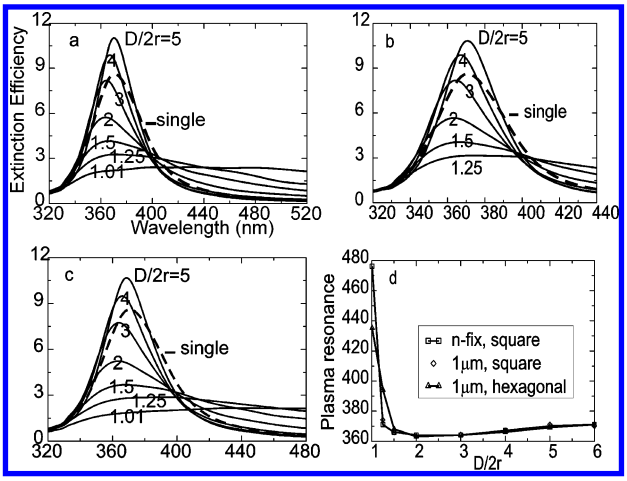

Figure 7. Variation of extinction for two-dimensional array of 30-nm spheres with different $D/(2r)$ obtained from coupled dipole calculation: (a) results for square structure, N fixed; (b) results for square structure, fixed array size; (c) results for hexagonal structure, fixed array size; (d) comparison of λ_{max} obtained for these three structures. Also included in each plot is the result for a single sphere. Note that a different wavelength scale is used in panels a−c.

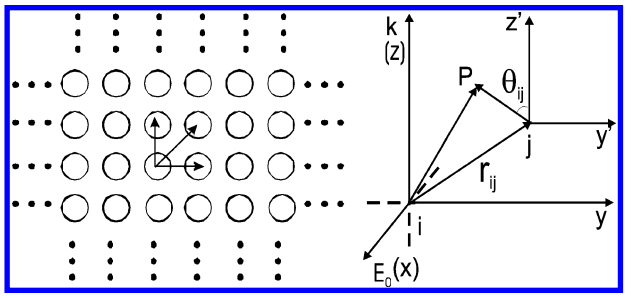

Figure 8. Structure of the two-dimensional infinite array and definition of the coordinate system. P is any observation point.

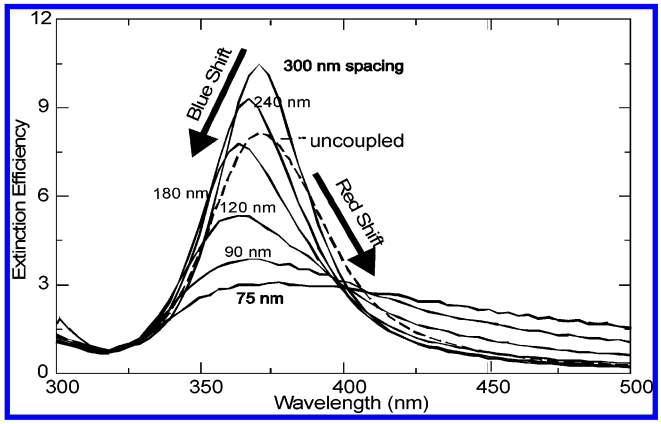

Figure 9. Extinction obtained from the semianalytical model for the two-dimensional infinite array of 30-nm spheres.

We now use eqs 12 and 13 to evaluate the extinction cross section for a two-dimensional array of 30-nm spheres. Here the dipole sums are evaluated using a sufficiently large array (800 × 800) that the sums are converged. A plot of the resulting efficiencies for different separation ratios is presented in Figure 9. Also plotted in this figure is the single-sphere or uncoupled extinction efficiency. Comparing Figure 9 with Figures 6b or 7b, we see that this semianalytical model gives similar results to the T-matrix method or CD approach.

Note that eq 12 shows that the retarded dipole sum S plays a crucial role in determining the variation of the plasmon band with array density. Indeed, Markel,[30] who performed an analysis similar to this for one-dimensional chains, has already shown

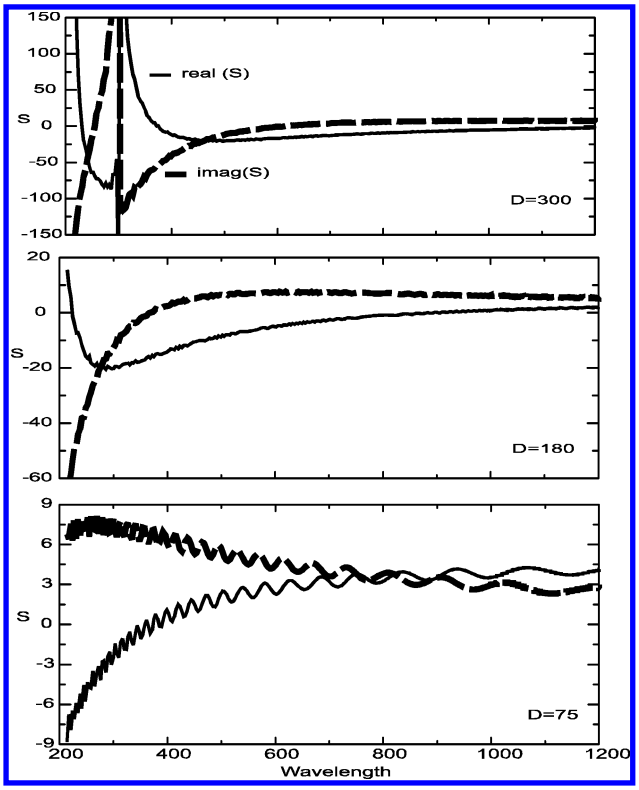

Figure 10. Plots of dipole sum vs wavelength for lattice spacing D = 300, 180, and 75 nm.

TABLE 1: The Dipole Sum *S*, Its Two Components, and the Corresponding Plasmon Width, γ_{array}, and Plasmon Resonance Wavelength, λ_{array}, for λ = 400 nm and γ = 0.44 eV

$D/(2r)$	S	$S(1/d^3)$	$S(1/d)$	γ_{array} (eV)	λ_{array} (nm)
5	−11.4 − 41.7i	−8.41 − 2.72i	−2.95 − 39.0i	0.36	370.39
3	−14.3 + 2.44i	−2.33 + 5.11i	−11.9 − 2.67i	0.498	363.43
1.25	1.09 + 6.14i	3.18 + 3.43i	−2.09 + 2.71i	1.25	377.34

that the real part of S (S_R) determines the plasmon resonance wavelength and its imaginary part (S_I) the plasmon width. Using a single-sphere plasmon wavelength and plasmon width (for a 30 nm sphere), we have calculated S as a function of wavelength with the array spacing D taken to be 300, 180, and 75 nm. The results are presented in Figure 10. Figure 10a shows that both S_R and S_I have large positive peaks for a wavelength that matches the array spacing. For wavelengths longer than D, S_R drops gradually to a negative minimum and then rises to a positive value in the static limit, while S_I drops quickly to a negative minimum, then rises to a positive value, and then ultimately goes to zero in the static limit. To understand the consequences of these results, in Table 1, we present specific values of S and the corresponding plasmon width changes and wavelength shifts for λ = 400 nm and γ = 0.44 eV. Here we see that for D = 300 nm, both S_R and S_I are negative, for D = 180 nm, S_R is still negative while S_I is now positive, while for D = 75 nm, both S_R and S_I are positive. Corresponding to the negative S_R and S_I, the plasmon wavelength blue shifts and the plasmon width narrows. In other words, going from 300 to 75 nm spacing, the plasmon width first narrows and then broadens, the switch in behavior occurring at 180 nm, while the plasmon wavelength first blue shifts and then red shifts, the switch in behavior occurring at 75 nm.

When these values of S are decomposed into electrostatic ($1/r^3$) and electrodynamic ($1/r$) components (also shown in Table

1), we see that the $1/r$ term is dominant in determining S_I for $D = 300$ nm but the $1/r^3$ term becomes more important for smaller D. The $1/r^3$ contribution plays a more important role in determining S_R, but otherwise the trends are the same. The wavelength at which the shift occurs is largely determined by the criterion $kD = 2\pi D/\lambda = 1$, which corresponds to where the interaction between dipoles switches from being dominated by electrostatic interactions to electrodynamic interactions. The optimal blue shifts and narrowing are found when S_R and S_I have their most negative values. This occurs when the array spacing is slightly smaller than the plasmon wavelength, which corresponds to detuning the dipole sums slightly from resonance such that long-range interactions and hence long-range radiative dipolar interactions are most important. By contrast, large red shifts and broadening occur when the array spacing is much smaller than the wavelength because S_R and S_I both are positive in that limit.

Note that the semianalytical model also tells us an important difference between one-dimensional chains and two-dimensional arrays. When applied to one-dimensional chains for the case of parallel polarization, eq 13 shows that the $1/r$ term vanishes (because all of the angles θ_{ij} are zero). This means that only the $1/r^3$ term contributes to the dipole sum, and this falls off more quickly than the $1/r$ term, so conditions that give rise to blue shifts and narrowing are much less important than they are for two-dimensional arrays. This explains why the plasmon wavelength for the case of parallel polarization in Figure 4 only shows red shifts. If we next consider the case of perpendicular polarization, θ_{ij} is now nonzero, so the $1/r$ term can now contribute. However in this case, the $1/r^3$ term already produces blue shifts, even at short range, so the additional blue shifts associated with the $1/r$ term are less noticeable. From these results, we see that long-range radiative dipolar interactions are less important for chains than they are for two-dimensional arrays.

IV. Conclusions

The primary goal of this work was to use the T-matrix and coupled dipole methods to characterize the extinction spectra of one-dimensional chains and two-dimensional arrays of silver nanoparticles with emphasis on spheres with a radius of 30 or 5 nm. We demonstrated that for an array spacing $D/(2r)$ greater than unity, the coupled dipole approach can describe array spectra accurately. The coupled dipole approximation can be improved as $D/(2r)$ approaches unity by choosing the array dimension to be smaller, but the optimal scaling does not agree with earlier estimates.

Much of our results involved characterizing the variation of the dipole plasmon resonance wavelength and width with particle size, array spacing, array symmetry, and polarization direction. Our results for one-dimensional chains show that as the spacing decreases, the plasmon width broadens under both parallel and perpendicular polarization but the wavelength mostly red shifts under parallel polarization and blue shifts under perpendicular polarization.

For two-dimensional arrays with polarization parallel to the plane, our results show that the plasmon resonance blue shifts as array spacing decreases for array spacings D larger than approximately 75 nm and then it red shifts for smaller spacings. The red shifts are in accord with what had been expected previously on the basis of static dipolar interactions, but the blue shifts (which by the way are not important for one-dimensional chains for parallel polarization) are a new result. In addition, the plasmon narrows as density is increased for $D > 180$ nm but broadens for smaller D. Our calculations also demonstrate that the array spectrum does not change much with array symmetry (square or hexagonal) or with measurement conditions (constant array size or constant particle number).

To explain the above optical behavior, we developed a semianalytical model based on the CD approximation for an infinite chain or two-dimensional array. Our calculations show that the plasmon wavelength shift is determined by the real part of the retarded dipole sum while the width change is determined by the imaginary part of this sum. For two-dimensional arrays, this theory shows that long range radiative dipolar coupling (which varies as $1/r$) is largely responsible for the blue shifts and narrowing seen for large particle separations while the short range ($1/r^3$) dipolar coupling leads to red shifts and broadening for small spacings. In addition, the optimal blue shifts and narrowing are found when the array spacing is slightly smaller than the plasmon wavelength, while red shifts and broadening can be found for spacings much smaller than the plasmon wavelength. The $1/r$ term plays a less important role for one-dimensional chains, and as a result, the plasmon wavelength shows a monotonic dependence on array spacing.

Acknowledgment. We acknowledge support of the Nanoscale Science and Engineering Initiative of the National Science Foundation under NSF Award Number EEC-0118025. Any opinions, findings, and conclusions or recommendations expressed in this material are those of the author(s) and do not necessarily reflect those of the National Science Foundation. Support was also provided by the Air Force Office of Scientific Research MURI program (Grant F49620-02-1-0381). We thank Anne Lazarides, Christy Haynes, Adam MacFarland, and Richard Van Duyne for valuable discussions.

References and Notes

(1) Mirkin, C. A.; Letsinger, R. L.; Mucic, R. C.; Storhoff, J. J. *Nature* **1996**, *382*, 607.
(2) Boal, A. K.; Ilhan, F.; DeRoucher, J. E.; Thurn-Albrecht, T.; Rotello, V. M. *Nature* **2000**, *404*, 746.
(3) Oldenburg, S. J.; Hale, G. D.; Jackson, J. B.; Halas, N. J. *Appl. Phys. Lett.* **1999**, *75*, 1063.
(4) Krenn, J. R.; Schider, G.; Rechberger, W.; Lamprecht, B.; Leitner, A.; Aussenegg, F. R.; Weeber, J.-C. *Appl. Phys. Lett.* **2000**, *77*, 3379.
(5) Kano, H.; Knoll, W. *Opt. Commun.* **2000**, *182*, 11.
(6) Somekh, M. G.; Liu, S.; Velinov, T. S.; See, C. W. *Appl. Opt.* **2000**, *39*, 6279.
(7) Tan, W.-C.; Preist, T. W.; Sambles, J. R. *Phys. Rev. B* **2000**, *62*, 11134.
(8) Tan, W.-C.; Sambles, J. R.; Preist, T. W. *Phys. Rev. B* **2000**, *61*, 13177.
(9) Jensen, T.; Kelly, L.; Lazarides, A.; Schatz, G. C. *J. Cluster Sci.* **1999**, *10*, 295.
(10) Draine, B. T.; Flatau, P. J. *J. Opt. Soc. Am. A* **1994**, *11*, 1491.
(11) Novotny, L.; Pohl, D. W.; Hecht, B. *Opt. Lett.* **1995**, *20*, 970.
(12) Taflove, A. *Artech House, Boston* **1995**, 599.
(13) Barber, P. W.; Hill, S. C. *Light Scattering by Particles: Computational Methods*; World Scientific: Singapore, 1990.
(14) Comberg, U.; Wriedt, T. *J. Quant. Spectrosc. Radiat. Transfer.* **1999**, *63*, 149.
(15) Wriedt, T. *Part. Part. Syst. Charact.* **1998**, *15*, 67.
(16) Weeber, J.-C.; Girard, C.; Krenn, J. R.; Dereux, A.; Goudonnet, J.-P. *J. Appl. Phys.* **1999**, *86*.
(17) Krenn, J. R.; Dereux, A.; Weeber, J.-C.; Bourillot, E.; Lacroute, Y.; Goudonnet, J.-P.; Schider, G.; Gotschy, W.; Leitner, A.; Aussenegg, F. R.; Girard, C. *Phys. Rev. Lett.* **1999**, *82*, 2590.
(18) Royer, P.; Goudonnet, J. P.; Warmack, R. J.; Ferrell, T. L. *Phys. Rev. B* **1987**, *35*, 3753.
(19) Foss, C. A.; Hornyak, G. L.; Stockert, J. A.; Martin, C. *J. Phys. Chem.* **1994**, *98*, 2963.
(20) Tomchuk, P. M.; Tomchuk, B. P. *J. Exp. Theor. Phys.* **1997**, *85*, 360.
(21) Hovel, H.; Fritz, S.; Hilger, A.; Kreibig, U. *Phys. Rev. B* **1993**, *48*, 18178.

(22) Kreibig, U.; Vollmer, M. *Optical Properties of Metal Clusters*; Springer-Verlag: New York, 1995; Vol. 25.
(23) Quinten, M.; Kreibig, U. *Appl. Opt.* **1993**, *32*, 6173.
(24) Taleb, A.; Petit, C.; Pileni, M. P. *J. Phys. Chem. B* **1998**, *102*, 2214.
(25) Taleb, A.; Russier, V.; County, A.; Pileni, M. P. *Phys. Rev. B* **1999**, *59*, 13350.
(26) Storhoff, J. J.; Lazarides, A. A.; Mucic, R. C.; Mirkin, C. A.; Letsinger, R. L.; Schatz, G. C. *J. Am. Chem. Soc.* **2000**, *122*, 4640.
(27) Schatz, G. C. *THEOCHEM* **2001**, *573*, 73.
(28) Murray, C. A.; Bodoff, S. *Phys. Rev. Lett.* **1984**, *52*, 2273.
(29) Kelly, K. L.; Lazarides, A. A.; Schatz, G. C. *Comput. Sci. Eng.* **2001**, *3*, 67.
(30) Markel, V. A. *J. Mod. Opt.* **1993**, *40*, 2281.
(31) Lazarides, A. A.; Schatz, G. C. *J. Phys. Chem. B* **2000**, *104*, 460.
(32) Haynes, C.; MacFarland, A.; Zhao, L. L.; Duyne, R. P. V.; Schatz, G. C.; Gunnarsson, L.; Kall, M. *J. Phys. Chem. B* **2003**, *107*, 7337.
(33) Borghese, F.; Denti, P.; Toscano, G.; Sidoni, I. O. *Appl. Opt.* **1979**, *18*, 116.
(34) Bruning, J. H.; Lo, Y. U. *IEEE Trans. Antennas Propag.* **1971**, *19*, 378.
(35) Fuller, K. A.; Kattawar, G. W. *Opt. Lett.* **1988**, *13*, 90.
(36) Hamid, A.-K. *J. Electromagn. Waves Appl.* **1996**, *10*, 723.
(37) Mackowski, D. W. *J. Opt. Soc. Am. A* **1994**, *11*, 2851.
(38) Waterman, P. C. *Phys. Rev. D* **1971**, *3*, 825.
(39) Mishchenko, M. I.; Travis, L. D. *Opt. Commun.* **1994**, *109*, 16.
(40) Mishchenko, M. I.; Mackowski, D. W.; Travis, L. D. *Appl. Opt.* **1995**, *34*, 4589.
(41) Mishchenko, M. I.; Travis, L. D.; Mackowski, D. W. *J. Quant. Spectrosc. Radiat. Transfer*. **1996**, *55*, 535.
(42) Mackowski, D. W.; Mishchenko, M. I. *J. Opt. Soc. Am. A* **1996**, *13*, 2266.
(43) Mackowski, D. W. *J. Quant. Spectrosc. Radiat. Transfer*. **2001**, *70*, 441.
(44) Lynch, D. W.; Hunter, W. R. In *Handbook of optical constants of solids*; Palik, E. D., Ed.; Academic Press: New York, 1985.
(45) Papavassiliou, G. C. *Prog. Solid State Chem.* **1979**, *12*, 185.
(46) Brongersma, M. L.; Hartman, J. W.; Atwater, H. A. *Phys. Rev. B* **2000**, *62*, 16356.
(47) Markel, V. A. *J. Mod. Opt.* **1992**, *39*, 853.
(48) Markel, V. A.; Shalaev, V. M.; Stechel, E. B.; Kim, W.; Armstrong, R. L. *Phys. Rev. B* **1996**, *53*, 2425.
(49) Russier, V.; Pileni, M. P. *Surf. Sci.* **1999**, *425*, 313.
(50) Chumanov, G.; Sokolov, K.; Cotton, T. M. *J. Phys. Chem.* **1996**, *100*, 5166.